



On the relationship between structure, morphology and large coseismic slip: A case study of the M_w 8.8 Maule, Chile 2010 earthquake



Eduardo Contreras-Reyes^{a,*}, Andrei Maksymowicz^a, Dietrich Lange^b, Ingo Grevemeyer^b, Pamela Muñoz-Linford^{a,c}, Eduardo Moscoso^d

^a Departamento de Geofísica, Facultad de Ciencias Físicas y Matemáticas, Universidad de Chile, Santiago, Chile

^b GEOMAR Helmholtz Centre for Ocean Research, Kiel, Germany

^c Universidad de Los Lagos, Puerto Montt, Chile

^d ERDBEBEN, Geophysical Prospecting Company, Valparaíso, Chile

ARTICLE INFO

Article history:

Received 8 May 2017

Received in revised form 19 August 2017

Accepted 21 August 2017

Available online 12 September 2017

Editor: P. Shearer

Keywords:

subduction zone earthquake

Chile

convergent margin

accretionary prism

Maule 2010 earthquake

ABSTRACT

Subduction megathrust earthquakes show complex rupture behaviour and large lateral variations of slip. However, the factors controlling seismic slip are still under debate. Here, we present 2-D velocity-depth tomographic models across four trench-perpendicular wide angle seismic profiles complemented with high resolution bathymetric data in the area of maximum coseismic slip of the M_w 8.8 Maule 2010 megathrust earthquake (central Chile, 34° – 36° S). Results show an abrupt lateral velocity gradient in the trench-perpendicular direction (from 5.0 to 6.0 km/s) interpreted as the contact between the accretionary prism and continental framework rock whose superficial expression spatially correlates with the slope-shelf break. The accretionary prism is composed of two bodies: (1) an outer accretionary wedge (5–10 km wide) characterized by low seismic velocities of 1.8–3.0 km/s interpreted as an outer frontal prism of poorly compacted and hydrated sediment, and (2) the middle wedge (\sim 50 km wide) with velocities of 3.0–5.0 km/s interpreted as a middle prism composed by compacted and lithified sediment. In addition, the maximum average coseismic slip of the 2010 megathrust event is fairly coincident with the region where the accretionary prism and continental slope are widest (50–60 km wide), and the continental slope angle is low ($<5^\circ$). We observe a similar relation along the rupture area of the largest instrumentally recorded Valdivia 1960 M_w 9.5 megathrust earthquake. For the case of the Maule event, published differential multibeam bathymetric data confirms that coseismic slip must have propagated up to \sim 6 km landwards of the deformation front and hence practically the entire base of the middle prism. Sediment dewatering and compaction processes might explain the competent rheology of the middle prism allowing shallow earthquake rupture. In contrast, the outer frontal prism made of poorly consolidated sediment has impeded the rupture up to the deformation front as high resolution seismic reflection and multibeam bathymetric data have not showed evidence for new deformation in the trench region.

© 2017 Elsevier B.V. All rights reserved.

1. Introduction

Accretionary convergent margins are typically characterized by slow convergence rate (<7.6 cm/a) and trench sediment thickness exceeding 1 km thick (e.g., Clift and Vannucchi, 2004). The outer part of their forearc presents a wedge shaped mass of accumulated sediment usually referred as the accretionary prism or accretionary wedge. This is the case of the south-central Chilean convergent

margin where tectonic accretion has dominated since at least the Pliocene (e.g., Kukowski and Oncken, 2006). In fact, seismic studies reveal the presence of a wedge body of reduced seismic velocities interpreted as an accretionary prism made of unconsolidated and semi-consolidated sediments (Contreras-Reyes et al., 2010; Moscoso et al., 2011). In this paper, we focus on the seismic structure of the central Chilean continental margin (34° – 36° S), and we present new and published seismic constraints for the structure of the accretionary prism using four trench-perpendicular wide angle seismic profiles covering a region of about 130×150 km².

The structural study of the accretionary prism is important because it has seismotectonics implications for controlling the updip

* Corresponding author.

E-mail address: econtreras@dgf.uchile.cl (E. Contreras-Reyes).

zone of interplate earthquakes in the shallow part of the subduction interface. Accretionary prisms are often thought to be aseismic and considered to be a barrier along dip for seismic rupture of interplate earthquakes (Byrne et al., 1988; Scholz, 1998; Saffer and Marone, 2003). In contrast, arcwards of the accretionary prism, the unstable stick-slip behaviour of the framework rock would promote seismic earthquake ruptures (e.g., Scholz, 1998; Wang and Hu, 2006). However, recent studies document evidence that coseismic rupture may occur up to the prism toe in accretionary margins. For example, ODP surveys off southern Japan in the Nankai subduction zone examined samples from the plate boundary fault at the toe of the accretionary prism. Geothermometry analysis reveals that this fault zone underwent temperatures higher than 380 °C suggesting that frictional heating occurred, and therefore coseismic slip must have propagated up to the deformation front likely during the 1944 and 1946 Nankai earthquakes (Sakaguchi et al., 2011). Another example, is the Sumatran subduction zone where high resolution seismic studies reported evidence for coseismic slip extending close to the trench during the 2004 Sumatra M_w 9.3 megathrust earthquake (Gulik et al., 2011). Gulik et al. (2011) suggest that the dewatering and lithification of sediments during accretion made them rheologically competent to enable seaward updip extension of coseismic slip. Likewise, seismic, tsunami, and seafloor observations suggest considerable coseismic slip up to the trench axis during the 2011 Tohoku-Oki earthquake M_w 9.1 in NE Japan (Simons et al., 2011; Fujiwara et al., 2011; Kodaira et al., 2012), albeit this margin has been classified as non-accretionary due to the absence of a well developed accretionary prism (e.g., Clift and Vanucci, 2004).

The M_w 8.8 Maule megathrust earthquake in central Chile on February 27, 2010 is characterized by two regions of high coseismic slip: a primary slip patch of 15–16 m north of the epicentre and a secondary maximum of 8–10 m in the southern part of the rupture area (e.g. Delouis et al., 2010; Lay et al., 2010; Lorito et al., 2011; Vigny et al., 2011; Moreno et al., 2012; Yue et al., 2014; Fig. 1). The two slip patches are the common features in the coseismic slip models presented by various studies, however, models differ in the location for the largest coseismic slip in the north. Some of the models locate the maximum coseismic slip near the trench (0–50 m) (Lay et al., 2010; Yue et al., 2014), others show moderate slip (6–8 m) near the trench (Vigny et al., 2011; Moreno et al., 2012; Delouis et al., 2010), and other coseismic slip models show the main slip patch 50–100 km from the trench with practically no slip in the trench region (Lorito et al., 2011; Lin et al., 2013; Fuji and Satake, 2013). Although some of these coseismic slip models incorporated tsunami records for their data inversion (actually the same data base), the differences reflect the poor resolution of coseismic slip close to the trench.

Maksymowicz et al. (2017) compared swath bathymetric data across the main slip path of the Maule event using data acquired before and after the Maule earthquake. Results show 3–5 m of coseismic uplift of the seafloor near the deformation front which is consistent with slip extending up to ~6 km landwards of the deformation front. This finding suggests that the interplate contact below the Maule accretionary prism can support seismic rupture near the trench during large earthquakes and has important implications for tsunamigenic processes. In order to better understand the interplay between the structure of the accretionary prism and coseismic slip on the shallow plate boundary fault, we studied the seismic structure of the accretionary prism complemented with high-resolution bathymetric data at the region of maximum coseismic slip of the 2010 Maule megathrust earthquake.

2. Tectonic setting and morphology of the central Chilean margin

Off central Chile, the oceanic Nazca plate subducts beneath the continental South American plate at a currently convergence rate of 6.6 cm/a with a convergence azimuth of N78°E (Angermann et al., 1999), although the convergence rate has decreased in about 40% during the last 20 Ma (DeMets et al., 2010). One of the most remarkable oceanic features off central Chile is the Juan Fernández Ridge (JFR); a hot spot track formed at the Juan Fernández hotspot located some 900 km west of the Chilean Trench. The current collision zone between the JFR and the Chilean margin at ~32.5°S has remained stationary since the last 10 Ma and is characterized by the presence of the Valparaíso Basin; a shelf forearc basin with ~3.0 km thick sediment fill of late Cenozoic age (Laursen et al., 2002). South of the JFR-trench collision zone, the trench fill is 1–2 km thick (e.g., Laursen et al., 2002), and sediment supply to the trench is mainly controlled by enhanced denudation of the Andean Cordillera during glaciation periods (e.g., Bangs and Cande, 1997). Hereafter, we refer to the region of the central Chilean margin between the JFR (~33°S) and the Mocha Fracture Zone (~38°S) as the Maule segment that is approximately coincident with the seismotectonic segment of the 2010 Maule earthquake rupture area.

Swath bathymetry data along the Maule segment were collected by the RV Sonne, RV Meteor, and RRS James Cook (Voelker et al., 2011; Maksymowicz et al., 2017). Bathymetric data show that the continental shelf and slope are indented by several submarine canyons that correspond to the offshore extension of the main rivers (Figs. 1 and 2). The width and slope of the continental shelf varies considerably along the Maule segment (20–50 km and 2°–30°, respectively) and its seaward edge is characterized by the shelf break at water depths in the range of 500–1500 m (Fig. 2). The shelf break is highlighted by the presence of v-shaped gullies reflecting the edge of the continental shelf exposed during glacial and interglacial period (Fig. 2A). The continental slope presents considerably variations along strike of its slope angle and width. Contreras-Reyes et al. (2016) described two sub-segments along the northern Maule segment: (1) the Mataquito sub-segment (34°–35.3°S) characterized by a smooth and wide continental slope with lower slope angle of 4°–5°, and (2) the Reloca sub-segment (35.3°–35.7°S) characterized by a relatively narrow and steep continental slope (lower slope angle of ~10° in average, Fig. 2). The most remarkable bathymetric feature along the Reloca sub-segment is the steep headwall scarp (up to 30°) and the mass wasting event (Reloca slide) at its base (Figs. 2 and 3; Contreras-Reyes et al., 2016). A comparison of bathymetric maps compiled before and after the Maule earthquake proves that no new major submarine landslide large enough to contribute significantly to the 2010 tsunami along the steep accretionary prism was identified (Voelker et al., 2011).

3. Seismic constraints

Seismic data were acquired off Maule in March 2008 during cruise JC23 of the British RRS James Cook. Here, we present the results of 2-D velocity depth-models of four wide-angle seismic profiles (Fig. 2). The 2-D velocity-depth models of lines P03 (Fig. 3A) and P09 (Fig. 3D) were already published by Moscoso et al. (2011) and Contreras-Reyes et al. (2016), respectively. In this paper, we include new results for profiles P01 and P02 obtained by joint inversion of refracted and reflected travel time arrivals (Korenaga et al., 2000). See the Supplementary Material for a description of the seismic experiment, seismic modelling, seismic data examples, and data fit. In this paper, we focus mainly on the seismic structure of the upper plate and subduction interface. The analysis of the

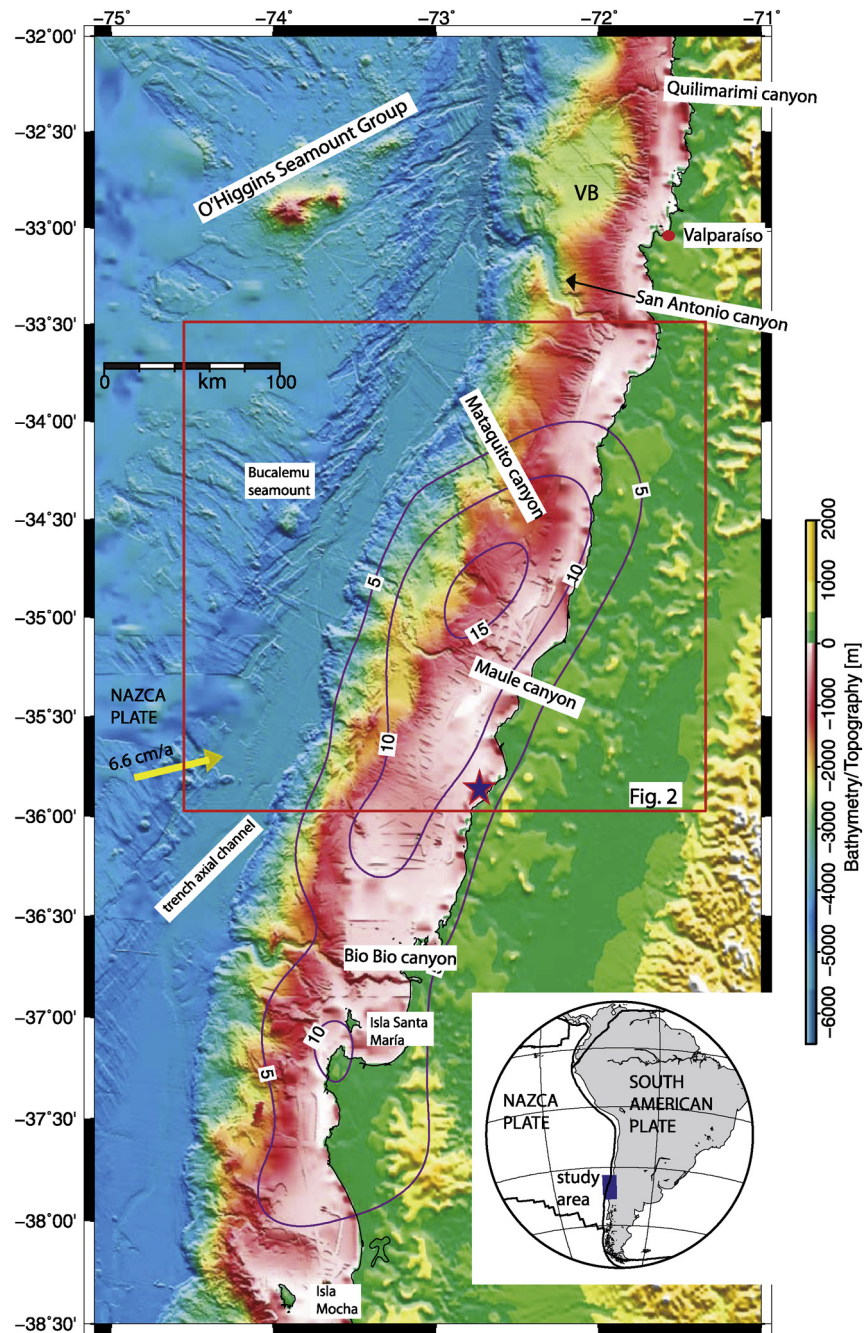


Fig. 1. Bathymetry of the seafloor based on high resolution multibeam data acquired aboard the RV SONNE, RV METEOR and RRS JAMES COOK (Voelker et al., 2011). The purple curves indicate the coseismic slip contours (in metres) of the Maule 2010 M_w 8.8 earthquake (Moreno et al., 2012) while the blue star indicates the 2010 mainshock epicentre determined by the Centro Sismológico Nacional de la Universidad de Chile. VB: Valparaíso Basin. (For interpretation of the references to colour in this figure legend, the reader is referred to the web version of this article.)

oceanic plate prior to subduction in the Maule segment was already discussed by Moscoso and Grevenmeyer (2015). Please note that lines P01–P03 lie in the Mataquito sub-segment, whereas P09 lies within the Reloca area.

The final 2-D velocity-depths models for profiles P01 and P02 are shown in Fig. 3C and 3B, respectively, and show typical sedimentary velocities for the forearc basin, trench fill, and outer part of the accretionary prism with P-wave velocity (V_p) values of 1.7–2.5 km/s. The velocity-depth models are also characterized by the presence of a wedge body with seismic velocities in the range of 1.7 and 5.0 km/s. Between 50 and 60 km landwards of the deformation front, a strong lateral velocity gradient is observed as an abrupt velocity increase from ~ 5.0 to ~ 6.0 km/s. Landwards of this

feature, velocities faster than 6.0 km/s increase more gradually. The main features of the velocity models presented here are similar to those found by Moscoso et al. (2011) along profile P03. However, there are morphological differences such as the width of the continental slope (Fig. 2) and sediment thickness within the forearc basin and slope apron. Seismic profile P09 is the shortest line where its landward termination locates few km seawards of the shelf break, and it crosses the Reloca Slide: a 24 km^3 mass wasting event. Along this line, the bathymetric profile presents an anomalously steep lower continental slope. Typical sedimentary velocities in the range of 2.0 and 4.5 km/s map the seaward part of the accretionary prism.

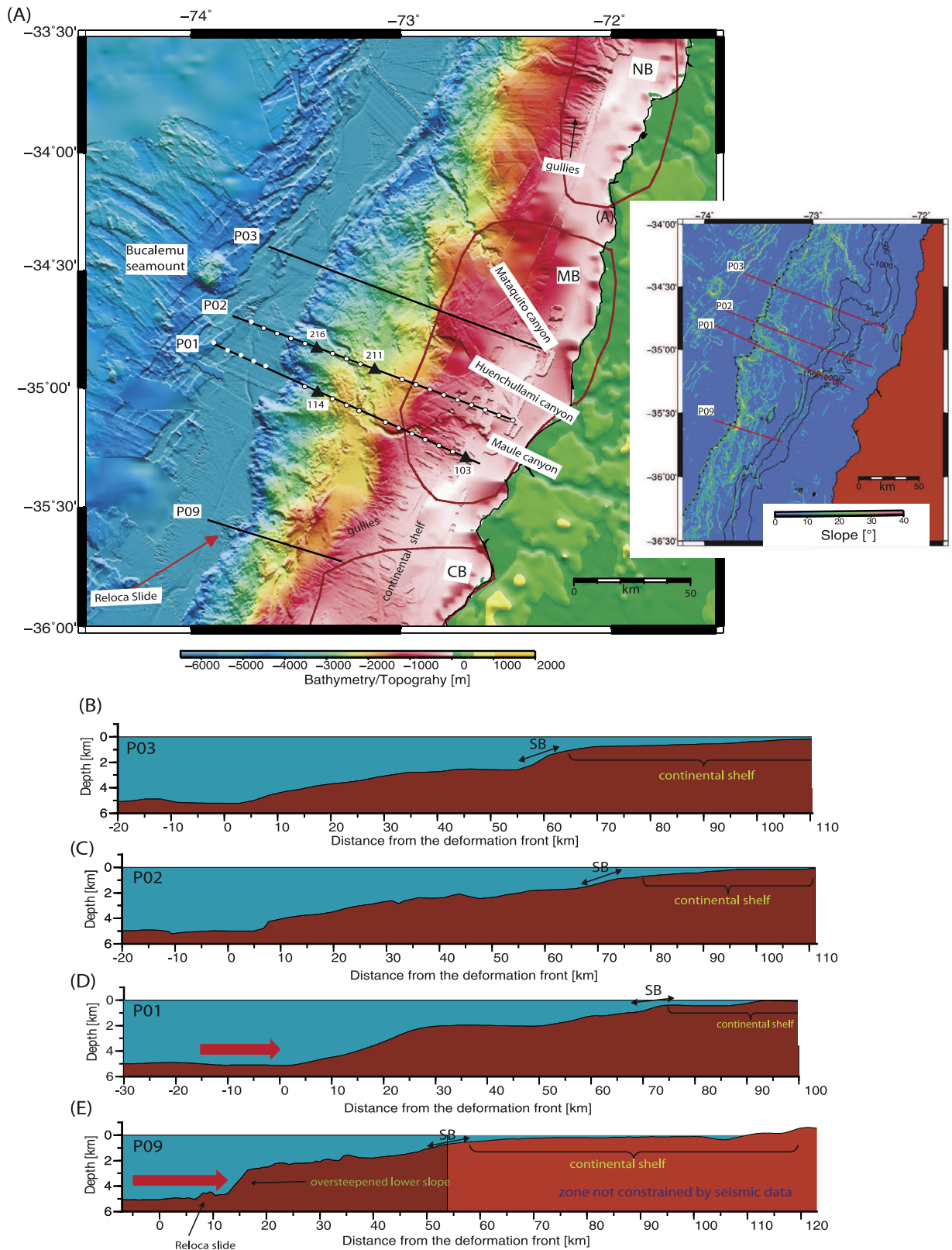


Fig. 2. (A) Bathymetric map of the O'Higgins and Maule districts of central Chile. Black lines denote the wide-angle seismic profiles studied by [Moscoso et al. \(2011\)](#), P03, [Contreras-Reyes et al. \(2016\)](#), P09; and this work, P01 and P02. The brown curves show the location of the forearc shelf basins (NB: Navidad Basin, MB: Mataquito Basin, and CB: Chanco Basin; e.g., [Contreras-Reyes et al., 2016](#)). Solid circles correspond to locations of OBH/S (Ocean Bottom Hydrophones/Seismometers) analysed in this study, while the black triangles indicate the station locations (see the Supplementary Material). Fault scarps are common along the seaward edge of the continental shelf (at the shelf break). The subpanel shows the slope of the marine forearc. The region defined by topographic contourlines of 500, 1000, and 1500 m are a good proxy for the location of the shelf break (SB) that is the transition from the relatively flat continental shelf to the continental slope. (B)–(D) Bathymetric profiles across the four seismic lines shown in (A). Note that the landward part of seismic profile P09 terminates near the SB. The red arrow indicates a local retreat of the deformation front across P01 and P09. Note the over-steepening of the lower continental slope across profiles P09 and P01. (For interpretation of the references to colour in this figure legend, the reader is referred to the web version of this article.)

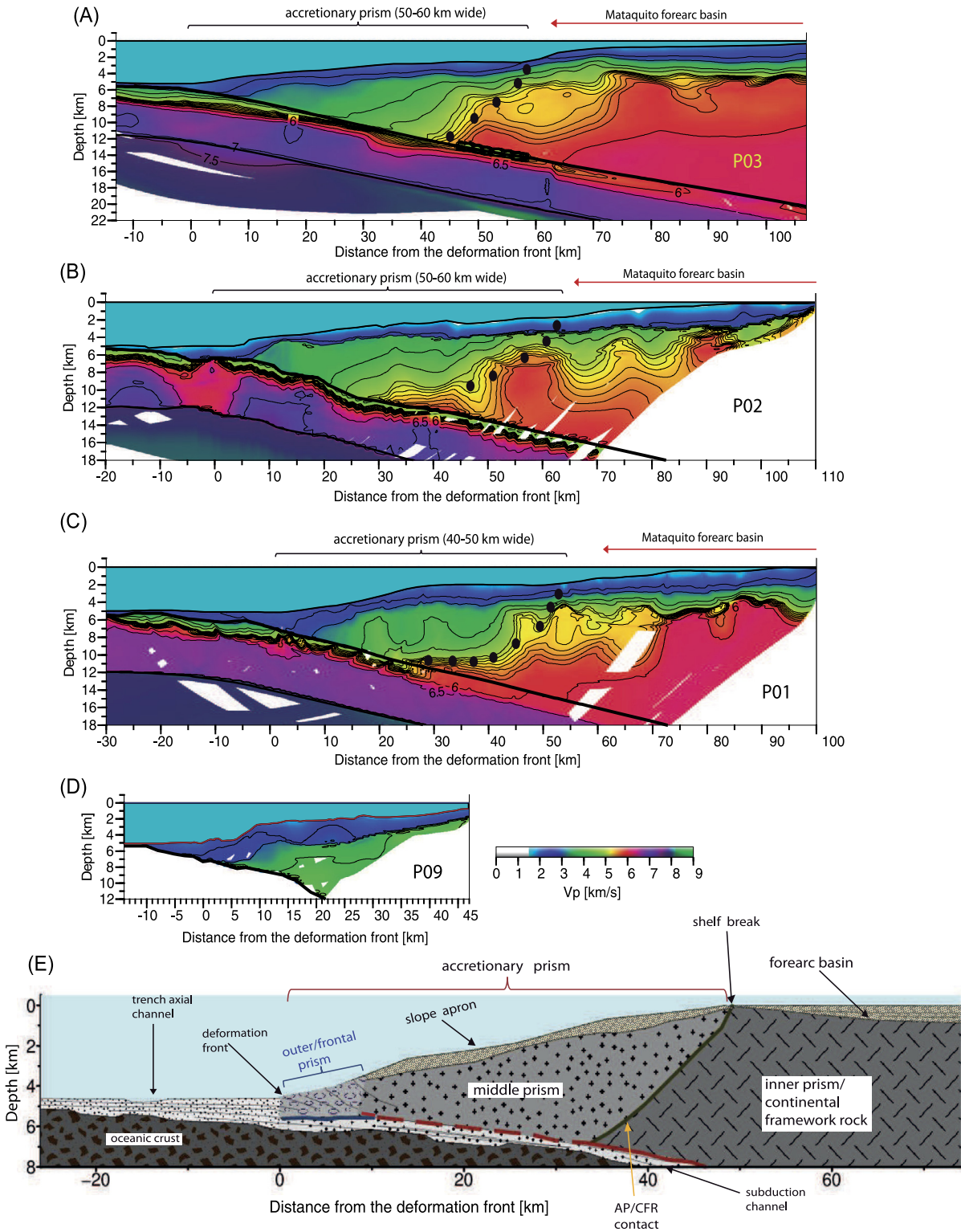


Fig. 3. (A–D) Direct comparison of the velocity models between profiles P3, P2, P1, and P9 (sorted from north to south, see Fig. 2A for map location). The landward edge of the accretionary prism is highlighted by black dots and it is defined by the abrupt lateral velocity gradient (not seen along P9 due to the lack of stations landwards of the shelf break, Fig. 2). For this study case, accretionary prism velocities are in the range of $1.8 \leq V_p \leq 5.5$ km/s. The shelf break is the surface expression of the lithological contact defined by the accretionary prism and continental framework rock. Unconsolidated sediments with typical velocities of 1.7–2.5 km/s define the sedimentary slope cover and the most seaward part of the accretionary prism as well as the trench fill. (E) Interpretative summary sketch based on knowledge of the Maule segment at different stages of the seismic cycle. The accretionary prism is composed by the outer/frontal prism (poorly consolidated sediment) and middle prism (more compacted and lithified sediment). The continental framework rock (or inner prism) corresponds to the paleo-accretionary prism or continental basement (Contreras-Reyes et al., 2010). The blue curves at the base of the outer/frontal prism indicates stable interseismic sliding frictional properties and velocity strengthening behaviour during the coseismic. The continuous red curve at the base of the inner prism denotes the unstable stick slip sliding. The more compacted and rigid sediment of the middle prism (relative to the frontal prism) promoted anomalous up dip trenchward extension of the Maule rupture area (dotted red curve) up to the outer/middle prism transition. The middle prism is characterized by a conditional stable behaviour during the interseismic and velocity-weakening behaviour during the coseismic. AP/CFR contact: Accretionary Prism/Continental Framework Rock contact or backstop. (For interpretation of the references to colour in this figure legend, the reader is referred to the web version of this article.)

4. Discussion/conclusion

4.1. Interpretation of seismic velocity models

The seismic lines P01–P03 sampled the seismic structure of the marine forearc from the deformation front up to few km seawards of the coast (Fig. 3). The three velocity-depth models show an abrupt lateral velocity gradient jumping from velocities of ~ 5.0 to ~ 6.0 km/s (black dots shown in Fig. 3A–C). This pronounced velocity contrast suggests a rock type change interpreted as the contact of the accretionary prism and the continental basement or framework rock ($V_p \geq 6.0$ km/s), and thus may represent the continental backstop. The superficial expression of this “seismic discontinuity” is approximately coincident with the slope-shelf transition. Thus, the continental slope is the superficial expression of the accretionary prism from the deformation front up to the shelf break. Across profile P03, the shelf break is cut by the Huenchullami canyon resulting in a vertical offset of about 1.5 km height (Figs. 2–4). This feature resembles an escarpment that separates the accretionary prism from the continental basement. Seismic line P01 crosses twice the Maule canyon (Fig. 2A), however, the walls of this canyon are significantly lower than those of the Huenchullami canyon resulting in a comparatively low vertical offset. The velocity-depth models along profiles P01–P03 show that the Mataquito forearc basin has a sedimentary unit of about 2 km thickness above the continental framework rock. The continental framework rock, or continental basement, onshore consists of metamorphic rocks attributed to the paleo-accretionary complex ($V_p > 6.0$ km/s) or western series (e.g., Glodny et al., 2006). The western series correspond with outcrops of a low-grade metapsammopelitic rocks with intercalations of metabasite derived from a late-Paleozoic accretionary prism.

The wedge shaped body with V_p values of 1.7 and 5.0 km/s located seawards of the seismic discontinuity highlighted in Figs. 3A–3C is interpreted as the accretionary prism off Maule. Seismic results along profiles P02 and P03 show a relatively large accretionary prism (50–60 km wide) beneath a smooth continental slope with a steady continental slope angle of $\sim 4^\circ$. Along line P01, the velocity model shows an accretionary prism of similar size (~ 50 km wide), however, the lower slope becomes steeper and the deformation front is shifted landward by ~ 10 km in relation to profiles P02 and P03. The middle and north continental slope is relatively uplifted and bounded in the north by the Maule canyon.

Fig. 3E summarizes our interpretation for the structure of the margin off Maule. The accretionary prism consists of two wedges: (1) the outer wedge or frontal prism (5–10 km wide) with seismic velocities of 1.8–3.0 km/s interpreted as a wedge of poorly compacted and hydrated sediment, and (2) the middle prism/wedge (10–50 km wide) with velocities of 3.0–5.0 km/s interpreted as a wedge made of more compacted and lithified sediment. Our seismic results show a continuous transition from the outer to the middle wedge suggesting that the young frontal prism merges into the older and more consolidated middle prism. Seismic velocities values of 3.0–5.0 km/s found here for the middle prism are similar to those found in erosive margins where usually the bulk rock of the eroded upper plate is igneous (von Huene et al., 2009). Thereby, the eroded and fractured framework rock structure mapped by seismic refraction data is difficult to distinguish from well lithified accreted sediment. However, multi-channel seismic reflection data acquired off Maule image imbricated thrust faults and folding structures and high degree of deformation of the middle prism (Contardo et al., 2008; Trehu and Tryon, 2012). Thus, we conclude a sedimentary origin for the middle prism off Maule. The greater velocities of the

middle prism compared to the frontal prism suggest a greater rigidity and more compacted sediment composition. The middle prism is bounded landward by the continental framework rock that consists of metamorphic basement. Wells et al. (2003) and Wang and Hu (2006) pointed out that the inner wedge or margin framework rock act as an apparent backstop and provided a stable environment for the formation of forearc basins. That is likely the case for the Maule margin that hosts the well developed Mataquito forearc basin containing up to 2 km of sediment infill (Fig. 3).

Based on the density-depth models of Maksymowicz et al. (2015), the V_p/V_s ratio models of Hicks et al. (2014), and the V_p models presented in this work, we computed representative values for the shear modulus G and Young's modulus E along the Maule margin. G and E describe the stiffness of the rocks, and the derivation of these elastic parameters is described in the Supplementary Material. Results show an abrupt increase of G and E values at the landward edge of the accretionary prism. This increase denotes a rheological contrast between the relatively weak middle prism ($G \sim 10$ GPa and $E = 20$ –30 GPa) and the stronger framework rock ($G > 15$ GPa and $E > 30$ GPa). On the trenchward side of the accretionary prism, the frontal prism is characterized by even lower values of G and E ($G \sim 5$ GPa and $E < 20$ GPa), which are consistent with poorly compacted and hydrated sediments (Fig. 3E). The framework rock, or continental basement, has a meta-sedimentary origin (the paleoaccretionary complex), whereas its trenchward edge defines the active backstop described by Contreras-Reyes et al. (2010) and Moscoso et al. (2011). Please note that the middle prism has a higher degree of consolidation and lithification than the frontal prism, but lower than the continental framework.

The landward retreat of the deformation front observed along P01 is a typical feature seen at convergent margins where seamounts subduct beneath the overriding plate causing compression and compaction in the frontal part of the collision zone accompanied by rapid subsidence at the back as the aftermath of seamount subduction (e.g., Dominguez et al., 2000). Maksymowicz et al. (2015) used gravimetric and magnetic data and detected the potential presence of a subducted seamount at $\sim (72.8^\circ\text{W}, 34.6^\circ\text{S})$ with a similar size of the Bucalemu seamount (Fig. 2A). However, the shape of the indentation of the lowermost continental slope along P01 does not match a theoretical entry trajectory of a seamount defined by the convergence direction of the Nazca and South American plates, which has an azimuth of about $N78^\circ\text{E}$ over the last 3 Ma (e.g., Angermann et al., 1999) which renders the hypothesis of seamount subduction unlikely.

Around profile P09, the lower continental slope is even steeper and the deformation front is shifted landwards up to 20 km in relation to profiles P02 and P03. Contreras-Reyes et al. (2016) proposed that the Reloca segment (around P09) is characterized by a lower continental slope that had reached an overcritical angle producing its failure and the spectacular mass wasting event (the Reloca slide). Likely, oversteepening of the lower slope is caused by basal accretion of subducted sediments, accompanied by high uplift rates (Contardo et al., 2008). Basal accretion and slope uplift is favoured by high basal friction at the plate interface (e.g. Kukowski and Oncken, 2006; Contardo et al., 2008) as have been proposed in the Reloca sub-segment by Cubas et al. (2013) and Maksymowicz et al. (2015) who used non-cohesive Coulomb wedge theory. For instance, Maksymowicz et al. (2015) estimated a long term effective basal friction coefficient μ_b of 0.47 for the Reloca sub-segment noticeably higher than the values estimated along the Mataquito sub-segment ($\mu_b = 0.36$) in the seawardmost part of the interplate contact.

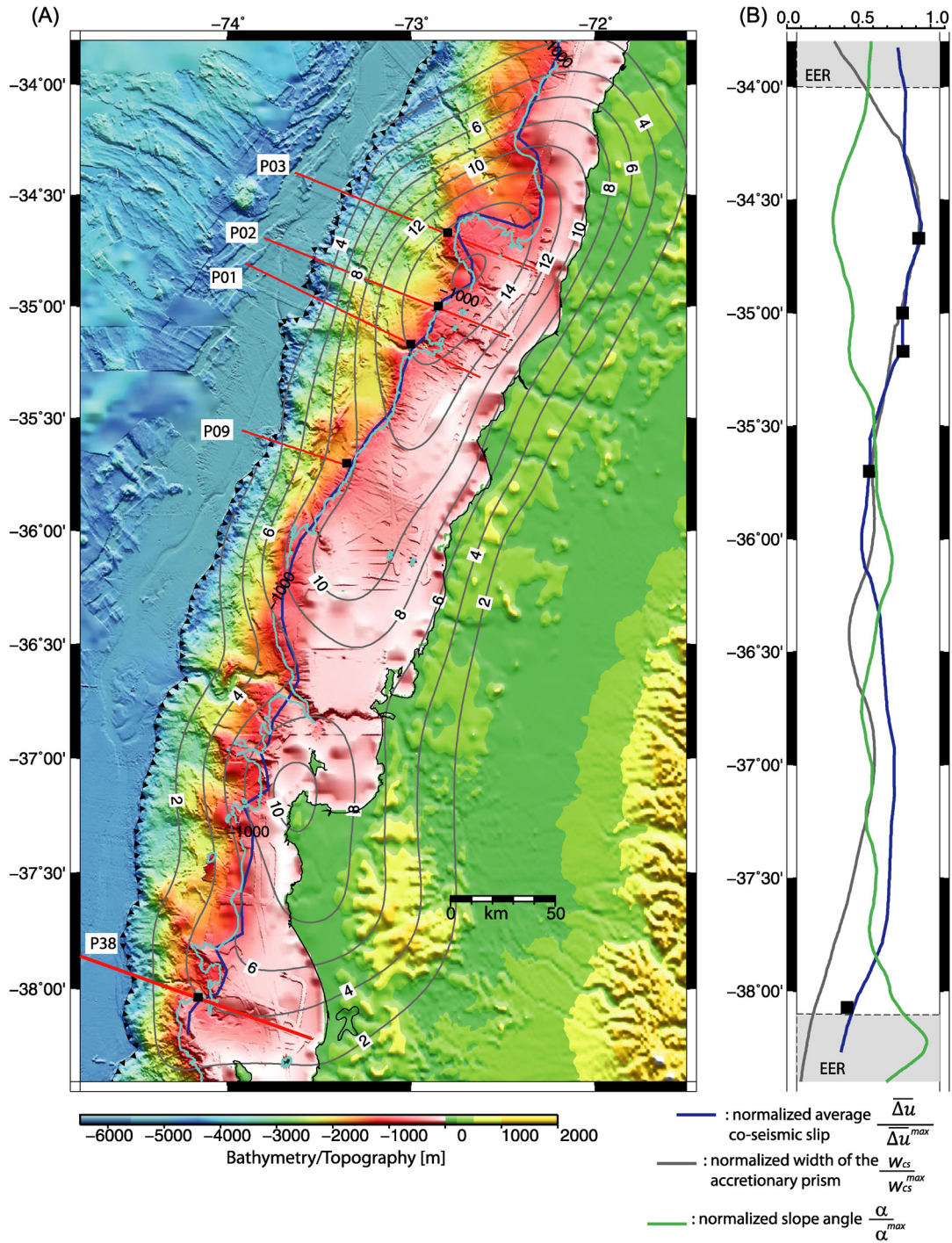


Fig. 4. (A) Rupture area of the Maule 2010 M_w 8.8 earthquake with high resolution bathymetric data. The gray curves indicate iso-contours of coseismic slip of the Maule earthquake (Moreno et al., 2012). Red lines denote the wide-angle seismic profiles P01–P03 and P09 presented in Fig. 2, whereas P38 corresponds to the seismic line studied by Contreras-Reyes et al. (2010). Black squares correspond to the superficial location of the accretionary prism/continental basement contact constrained by the seismic refraction data that is also coincident with the shelf break location. (B) The normalized coseismic slip $\frac{\Delta u}{\Delta u^{max}}$ averaged along tracks perpendicular to the trench axis (gray curve) is shown as well as the normalized width of the continental slope $\frac{w_{cs}}{w_{cs}^{max}}$ (blue curve). The normalized slope angle values $\frac{\alpha}{\alpha^{max}}$ are defined by the green curve and are taken from Maksymowicz (2015). Black squares indicate the width of the accretionary prism constrained by the seismic lines (red curves shown in A). Note the spatial correlation between low slope angle values and high average coseismic slip. The numeric values are $\Delta u^{max} = 7$ m, $w_{cs}^{max} = 72$ km, and $\alpha^{max} = 7^\circ$. EER: End of Earthquake Rupture. A median filter of 23 points was applied to the $\frac{\alpha}{\alpha^{max}}$ curve in order to remove high frequencies and highlight the long wavelength trend. (For interpretation of the references to colour in this figure legend, the reader is referred to the web version of this article.)

Along profile P09, the accretionary prism is presumably smaller, though, its landward edge is unconstrained by the lack of seismic stations along the continental shelf (Figs. 2 and 3). Nevertheless, 2-D density-depth models show that the shelf break de-

limit a wedge body of reduced densities in the region of line P09 (Maksymowicz et al., 2015). This suggests that the shelf break is a good indicator or proxy for the landward edge of the accretionary prism in the study area in agreement with the results

found along profiles P01–P03. Furthermore, seismic studies carried out at the northern and southern parts of the Maule segment: off Valparaíso at $\sim 33^\circ\text{S}$ (e.g., Zelt, 1999) and off Arauco Peninsula at $\sim 38.2^\circ\text{S}$ (Contreras-Reyes et al., 2010), respectively, document that the superficial location for the landward edge of the accretionary prism match the position of the shelf break. Therefore, we interpolate the superficial location for the landward edge of the accretionary prism as the shelf break along the entire Maule segment (Fig. 4). Nonetheless, in general the landward edge of the accretionary prism is not necessarily located below the shelf break. In fact, seismic refractions studies document that the landward edge of the accretionary prism off southern Chile (43° – 45°S) is placed near the deformation front along the lower continental slope (Fig. 5; Contreras-Reyes et al., 2010). Thus, our assumption that the shelf break is a good proxy for the landward edge of the accretionary prism along the Maule segment (33° – 38.5°S) is solely based on the seismic constraints of this particular area. This result will be used to quantify the size of the accretionary prism along strike and discuss its interplay with the Maule earthquake rupture area in the sub-section 4.3.

The 2-D velocity-depth models shown in Fig. 3 present a middle prism, ~ 50 km wide, defined by V_p values of 3.0–5.0 km/s, and a small frontal prism (< 10 km wide) defined by seismic velocities < 3.0 km/s. In contrast, the southern region of the Maule segment (around profile P38 shown in Fig. 4) is characterized by a wider frontal prism (20–25 km wide) below the continental slope whereas the middle prism trenchward of the shelf break is absent (see Supplementary material and Contreras-Reyes et al., 2010). The smaller frontal prism in the north can be explained by a decreased rate in sediment accretion in the northern part of the Maule segment (34° – 35.5°S) due to the decrease in the sediment supply to the north (Laursen et al., 2002). Alternatively, the middle prism becomes wider to the north, as is accommodated by the landward shift of the framework rock approaching the high trench and shoreline curvatures near the collision zone between the Juan Fernández Ridge and the continental plate. This is likely an important factor controlling the along strike variations in the morphology and size of the frontal and middle prisms.

4.2. The updip aseismic–seismic transition zone

The region characterized by an abrupt lateral velocity gradient and interpreted as the contact between accreted sediment and the continental framework rock has been classically referred as the backstop. This zone is rheologically stronger than the accretionary prism made of unconsolidated and semiconsolidated sediments (e.g., Byrne et al., 1988; Wells et al., 2003; Moscoso et al., 2011). Thus the base of the accretionary prism is expected to be compatible with stable slip and aseismic deformation and the backstop should control the transition between stable and stick-slip frictional sliding in the updip zone for large earthquakes (Byrne et al., 1988; Moscoso et al., 2011). Likewise, Wang and Hu (2006) proposed that the actively deforming outer wedge overlies the updip velocity-strengthening part of the subduction fault, and the strong inner wedge overlies the velocity-weakening part (the seismogenic zone). They also pointed out that the updip limit of the seismogenic zone must be transitional and mineralogical, hydrological, and thermal dependent. They further recognized that the outer wedge is not perfectly plastic and are capable of storing elastic strain energy in its stable regime.

Pietrzak et al. (2007) studied the source region of the 2004 Sumatra M_w 9.2–9.3 earthquake using GPS, altimeters, tide gauges and tsunami models. The results show that slip during the 2004 Sumatra event propagated updip, extending unusually close to the deformation front and reaching values of up to 20 m. The

upper subduction zone of Sumatra is well recognized as an accretionary margin (e.g., Clift and Vannucchi, 2004) with a massive accretionary prism complex composed of a frontal prism and a fossil accretionary domain (total width of > 110 km; Kopp et al., 2002). Gulick et al. (2011) used high resolution seismic constraints and image coherent sedimentary blocks with strong internal cohesion in this accretionary complex. They further interpreted the competent and strong rheology of the accretionary prism in terms of dewatering and lithification processes, which enabled rupture to propagate close to the Sunda Trench.

Another example for possible evidence of earthquake rupture near the trench in an accretionary margin is off SW Japan, where geothermometry data shows that coseismic slip must have propagated up to the toe of the accretionary prism likely during the 1944 and 1946 Nankai earthquakes (Sakaguchi et al., 2011). However, none of the mentioned studies (neither for the Sumatra nor the Nankai events) have provided direct evidence where coseismic fault slip reached the toe of the accretionary prism causing new deformation. Probably the most clear direct evidence for coseismic fault rupture all the way up to the trench was presented by Kodaira et al. (2012) using high resolution seismic reflection and bathymetry data acquired before and after the 2011 Tohoku-oki megathrust earthquake (M_w 9.1 off NE Japan). They detected a new deformed sedimentary layer 3 km long and 350 m thick indicating that fault rupture during the Tohoku-oki earthquake did reach the seafloor at the trench axis. Additional evidence for seismic slip in the trench region of this event is provided by comparison of multibeam bathymetry acquired before and after the event (Fujiwara et al., 2011). Thus it was concluded that the shallow plate interface at the subduction trench axis can slip seismically in the NE Japanese margin (Fujiwara et al., 2011; Kodaira et al., 2012). Because the NE Japanese margin is a largely recognized non-accretionary margin (e.g., Clift and Vanucci, 2004) and the considerably high slip in the trench region during the 2011 M_w 9.1 Tohoku-oki event (~ 50 m according to Simons et al., 2011), this case is not comparable with the 2010 M_w 8.8 event occurred in the accretionary Maule margin.

Maksymowicz et al. (2017) differentiated bathymetric tracks and mapped changes in the seafloor topography from before and after the Maule earthquake. The results show a significant difference close to the trench with 3–5 m of seafloor uplift landwards of the accretionary prism toe. This result is compatible with coseismic slip extending up to 6 km landwards of the deformation front, and implies that slip must have propagated along the entire base of the middle prism, but not necessarily up to the deformation front (Maksymowicz et al., 2017). In fact, the comparison of seismic reflection acquired before (Contardo et al., 2008) and after (Trehu and Tryon, 2012) the Maule earthquake do not present evidence of new deformation around the trench region (Maksymowicz et al., 2017), which renders the idea of important coseismic slip up to the deformation front unlikely. Hence, we propose that the transition from the frontal prism (5–10 km wide) to the middle prism (40–50 km wide) should control the updip limit of the coseismic rupture for the Maule event.

The location of the frontal to middle prism transition depends mainly on sediment composition, amount of lithification and dehydration processes. This transition would define a rheological boundary separating the frontal prism (that presents velocity weakening during the coseismic period) from the middle prism (that presents stable sliding behaviour during the interseismic period, but it is characterized by velocity-strengthening during the coseismic period). Then, the relatively high rigidity of the middle prism made of more compacted sediment (sandwiched between

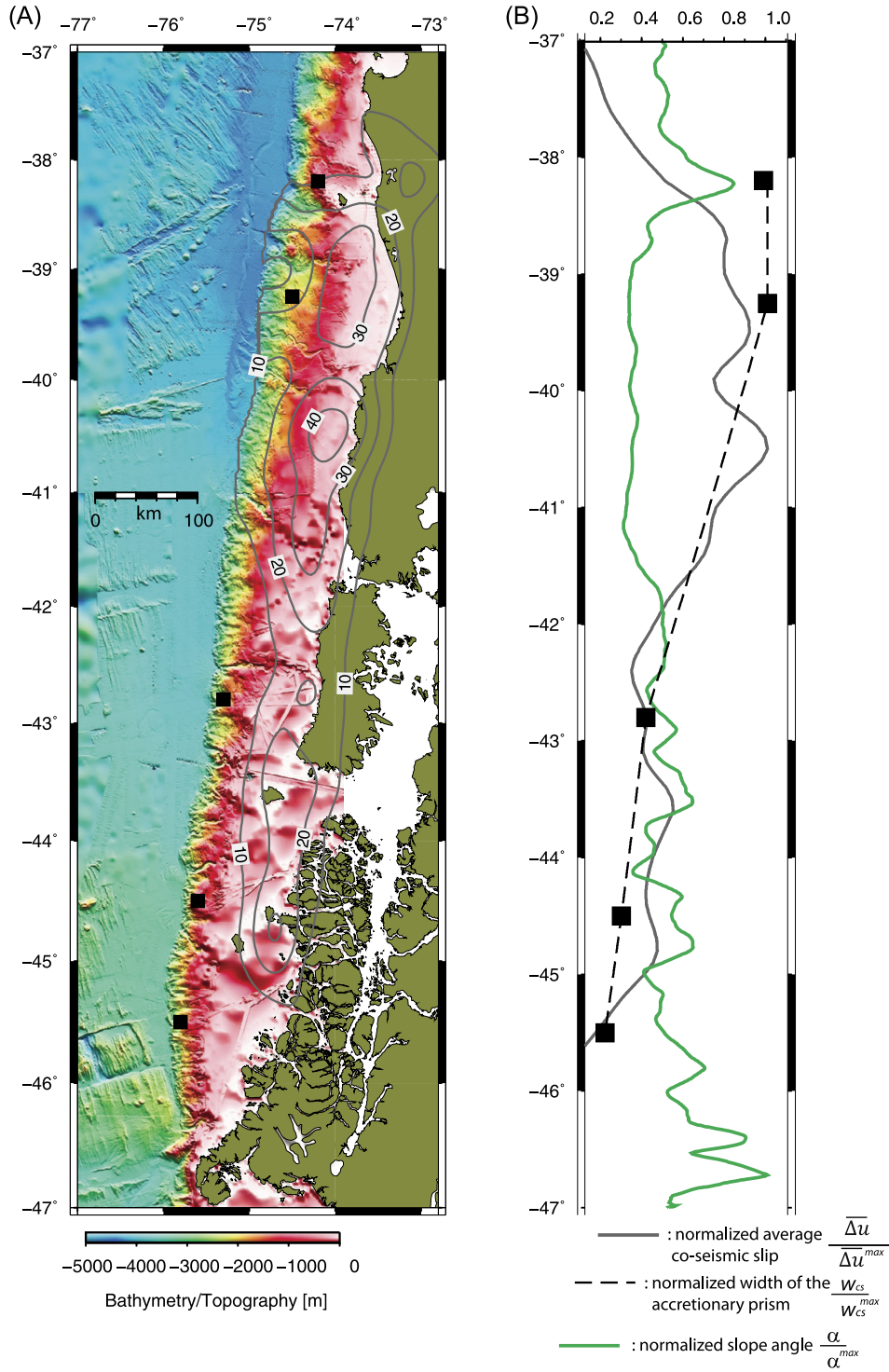


Fig. 5. (A) Rupture area of the Valdivia 1960 M_w 9.5 giant earthquake with high resolution bathymetric data. The red curves indicate iso-contours of coseismic slip of the Valdivia earthquake (Moreno et al., 2009). Purple squares denote the location of the landward edge of the accretionary prism based on seismic constraints (Bangs and Cande, 1997; Contreras-Reyes et al., 2010). (B) The normalized coseismic slip $\frac{\overline{\Delta u}}{\Delta u^{max}}$ averaged along tracks perpendicular to the trench axis (gray curve) is shown as well as the normalized width of the accretionary prism $\frac{w_{ap}}{w_{ap}^{max}}$ (dotted curve). The normalized slope angle values $\frac{\alpha}{\alpha^{max}}$ are defined by the green curve and are taken from Maksymowicz (2015). Note the spatial correlation of low slope angle values and high average coseismic slip. The numeric values are $\overline{\Delta u}^{max} = 13$ m, $w_{ap}^{max} = 27$ km, and $\alpha^{max} = 8^\circ$. A median filter of 23 points was applied to the $\frac{\alpha}{\alpha^{max}}$ curve in order to remove high frequencies and highlight the long wavelength trend. (For interpretation of the references to colour in this figure legend, the reader is referred to the web version of this article.)

the outer frontal and inner prisms) allowed further trenchward propagation of the Maule 2010 rupture to the base of most of the accretionary prism. In the following sub-section, we discuss

the along strike variations of this seaward-shifted updip limit that is spatially related to the transition from the frontal to middle prism.

4.3. Response of the accretionary prism during the coseismic motion of the Maule event

As we discuss above, most of the plate boundary interface at the base of the middle prism must have slipped seismically in the northern part of the Maule earthquake rupture area. It would be interesting to explore the trend and interplay between the size of the accretionary prism and the slip amount along the entire Maule 2010 rupture area. Fig. 4A shows the approximated location of the shelf break along the Maule earthquake rupture area (blue curve). This curve is extracted from the multibeam bathymetric data and it corresponds to the transition from the relatively flat continental shelf to the continental slope that is coincident with the region bounded by the iso-contour depth of approximately 1000 m (Fig. 2). Now, we can compute the width of the continental slope w_{cs} as the distance calculated orthogonally from the deformation front to the shelf break. As we discussed in the sub-section 4.1, w_{cs} is a good proxy for the width of the accretionary prism along the Maule earthquake rupture area. Fig. 4B shows the latitudinal variation for the normalized width of the continental slope w_{cs} . The maximum values of w_{cs} are located between 34.5° and 35.5°S, which is the area of maximum coseismic slip of the Maule event. In order to show that this observation is independent on whether the earthquake rupture reached the trench or not, we calculate the horizontal coseismic slip $\overline{\Delta u}$ averaged along tracks perpendicular to the deformation front for a length L_x as

$$\overline{\Delta u} = \frac{1}{L_x} \int_0^{L_x} \Delta u(x) dx \quad (1)$$

where the length L_x is taken from the deformation front up to the seawardmost distance where the coseismic slip $\Delta u(x)$ vanishes (usually 10–20 km landwards of the shore line as is shown in Fig. 4A). Fig. 4B shows the normalized computed values for $\overline{\Delta u}$ along the entire Maule rupture area. We also plot the normalized slope angles α of the continental slope (averaged from the deformation front up to the shelf break; Maksymowicz, 2015). $\Delta u(x)$ values were extracted from the coseismic slip model of Moreno et al. (2012), which is based on GPS and InSAR observations and includes a curved slab geometry. The location for the maximum values of $\overline{\Delta u}$ at the north of the epicentre should be a stable feature as most of the published coseismic slip models show the maximum slip between 34.5° and 35.5°S (Lay et al., 2010; Vigny et al., 2011; Delouis et al., 2010; Lorito et al., 2011; Lin et al., 2013; Yue et al., 2014).

Fig. 4B shows that the high average coseismic slip along the northern patch (34.5°–35.5°S) spatially correlates with the area where the accretionary prism is widest ($w_{cs} = 50$ –60 km). A similar pattern is seen in the secondary maximum coseismic slip at the southern part of the rupture area around 37°S. High values of $\overline{\Delta u}$ are also coincident with regions of low continental slope angles (Maksymowicz, 2015). The coseismic slip is relatively lower between 36° and 37°S where the continental slope and accretionary prism are deeply incised by the Bío-Bío canyon and there is no direct correlation between $\overline{\Delta u}$ and w_{cs} . Naturally, there is no correlation between $\overline{\Delta u}$ and w_{cs} at the northern and southern edges of the coseismic slip model where the earthquake rupture terminated (see Supplementary Material for further details on the computation of correlation coefficient values between the variables $\overline{\Delta u}$, w_{cs} , and the slope angle α).

The results shown in Fig. 4 are also consistent with the mechanically stable areas beneath the continental shelf surrounded with critical areas beneath the continental slope found by Cubas et al. (2013) who used critical taper theory constrained by topographic data. Their estimated stable areas coincide with the location of the rupture area and low effective basal friction coefficients

defining the seismogenic zone (Lin et al., 2013; Cubas et al., 2013). We repeated the analysis for the $M_w = 9.5$ 1960 Valdivia megathrust earthquake (e.g., Moreno et al., 2009) (Fig. 5). Since the slip inversion from Moreno et al. (2009) is based on land-level changes (Plafker and Savage, 1970) measured 8 years after the 1960 main-shock the coseismic model likely includes significant afterslip and the coseismic model is not comparable in quality as the 2010 earthquake, particularly south of 42°S. For the northern part of the 1960 rupture zone regions of maximum coseismic slip again correlate with low values of α and relatively large accretionary prisms. The Valdivia event ruptured across six major oceanic fracture zones covering a length of ~1,000 km from the Mocha Island in the north up to the CTJ in the south. Nevertheless, more seismic data are needed to confirm the correlation between high coseismic slip with wide accretionary prisms and low continental slope angles along the large rupture area of the Valdivia earthquake.

Apparently the spatial correlation between maximum coseismic slip and widest accretionary prism in the northern patch of the Maule event is related to the large size of the middle prism (40–50 km wide). As we discussed above, the more compacted and consolidated sediment of the middle prism may have facilitated shallow rupture of the Maule earthquake. Compaction and dewatering is expected to increase landward of the middle prism in agreement with the progressively increase in seismic velocities within the middle prism (Fig. 3). Compaction and dewatering of the accretionary prism could result in the trenchward migration of the unstable boundary (characterized by stick-slip behaviour), and therefore extend coseismic rupture as was the case for the Sumatra 2004 M_w 9.3 earthquake (Gulik et al., 2011). Alternatively, if the base of the middle prism is characterized by aseismic sliding during the interseismic period, velocity weakening behaviour can be induced by strong coseismic rupture associated to an earthquake nucleated in a deeper unstable zone (e.g., Wang and Hu, 2006). Consistently, the near-trench slip and observed outer rise seismicity can be seen as a direct consequence of the stress transferred from highest coseismic slip patch of the Maule event (Yue et al., 2014; Figs. 4 and 6).

Based on the results of bathymetric and seismic reflection data (acquired before and after the 2010 earthquake; Maksymowicz et al., 2017) the rupture of the Maule event probably did not reach the toe of the accretionary prism (contra Yue et al., 2014, who inverted a coseismic slip model with rupture extended up to the trench axis with a peak value >12 m). The outermost part of the accretionary prism (the frontal prism composed by poorly consolidated sediment) should have a velocity strengthening rheology or stable sliding behaviour. In this case, the updip segment of the plate boundary is instantaneously loaded by the rupture of the earthquake further downdip, but the dynamic strength of the frontal prism must increase to resist slip and generated coseismic compressional deformation inside the wedge (e.g., Wang and Hu, 2006). It is also worth-noting that most of the published coseismic slip models do not incorporate splay faults activated in some segments of the rupture zone of the Maule earthquake. Wang and Hu (2006) pointed out the relevance of splay faults in the amplification in the vertical component of coseismic slip to enhance tsunami generation. Lieser et al. (2014) used aftershocks of the Maule 2010 earthquake from an amphibious seismological network and resolve seismically active splay faulting landward of the accretionary prism in the area of maximum coseismic slip of the Maule event (northern patch). During the coseismic, however, high resolution data do not show evidence for splay faulting activation (Maksymowicz et al., 2017).

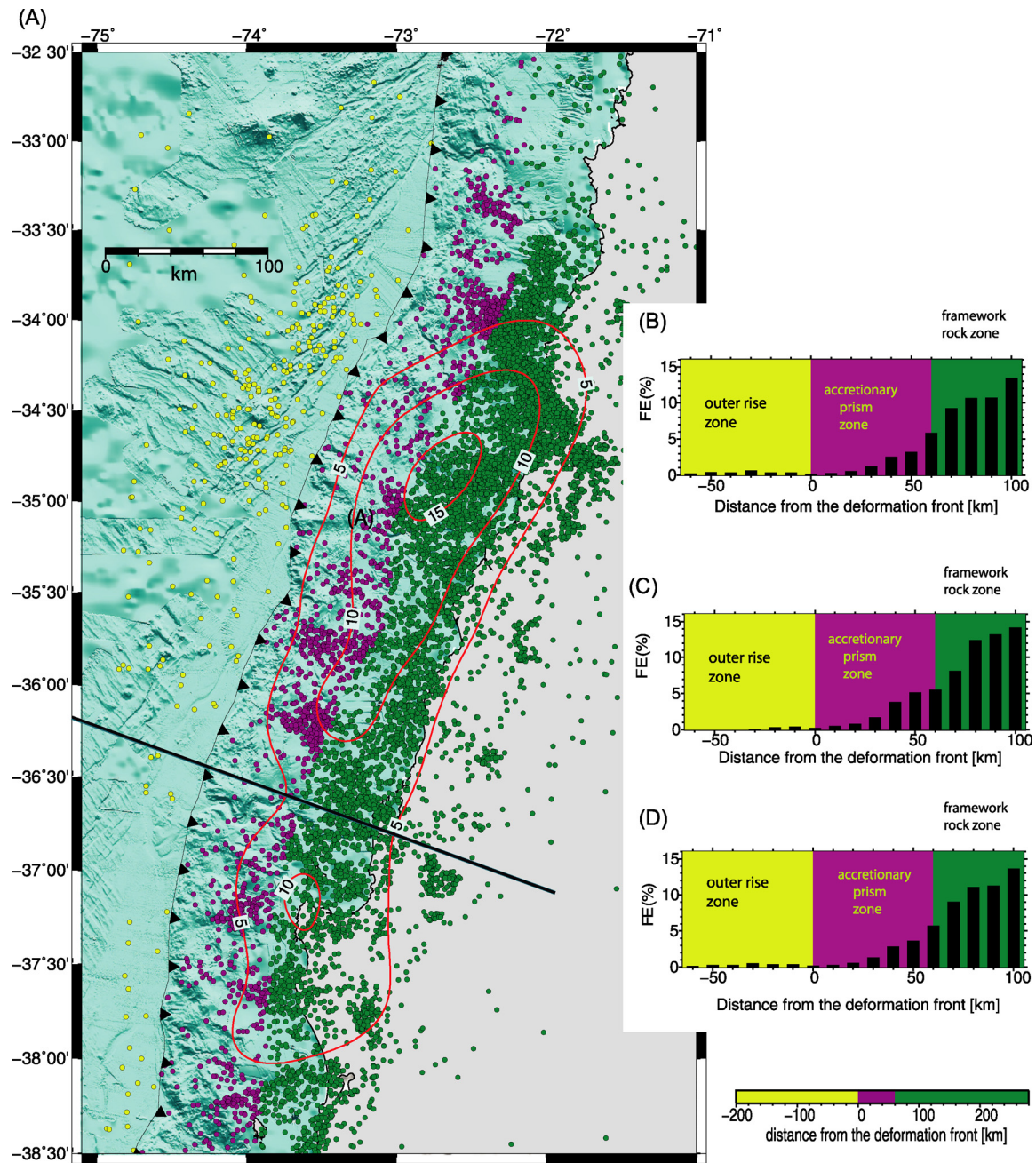


Fig. 6. (A) Aftershocks distribution between March 15 and September 30, 2010 of the Maule earthquake (Lange et al., 2012). Aftershocks are classified in three types: (1) outer rise events (yellow circles), (2) events occurred in the accretionary prism domain or within ~ 60 km from the deformation front (purple circles), and (3) events occurred beneath the continental framework rock zone (green circles). Coseismic slip distribution of the 2010 Maule event from Moreno et al. (2012) is shown with red contourlines in metres. Aftershocks shown have a moment magnitude > 3.5 . Note the scarce aftershock seismicity and reduced amount of coseismic slip along the continental slope surrounded by the Bio-Bio canyon. (B) Histogram with the number of aftershocks located in the area of the northern coseismic slip patch (i.e., north of the black line shown in (A)), (C) Histogram with the number of aftershocks located in the area of the southern coseismic slip patch (i.e., south of the black line shown in (A)), and (D) Histogram of all aftershocks in per centil. FE: frequency of earthquakes. (For interpretation of the references to colour in this figure legend, the reader is referred to the web version of this article.)

4.4. Response of the accretionary prism during the early postseismic period of the Maule event

Fig. 6 shows the aftershock seismicity recorded during the first semester after the Maule main shock using a local onshore network (Lange et al., 2012). Most of the events ($\sim 90\%$) are concentrated in the continental framework rock zone, landward of the middle prism. In particular, scarce aftershock seismicity lies just updip of the high slip patches. This result is also consistent with those found by Hicks et al. (2014) and Lieser et al. (2014) who used offshore local networks. Thus, both the frontal

and middle prisms behaved aseismic during the early postseismic period. A similar postseismic response of the outer forearc in the rupture area of the 2011 Tohoku-Oki megathrust earthquake was reported by Shinohara et al. (2012). In that case, the shallow portion of the interplate boundary presents considerable coseismic slip (Simons et al., 2011), but does not show significant postseismic activity (Shinohara et al., 2012). Rietbroek et al. (2012) and Hicks et al. (2014) pointed that the aftershocks concentrated in the areas of rapid transition from high to low slip. The absence of aftershock activity is not a particular feature of the shallow part of the plate boundary, but it has been observed where large slip was

estimated in the rupture areas of main shocks such as the case of the Tohoku-Oki, Sumatra, and the Illapel (central Chile) 2015 M_w 8.1 earthquakes (Shinohara et al., 2012; Tilmann et al., 2010; Lange et al., 2016) as well as the Maule earthquake (Lange et al., 2012, 2014; Rietbrock et al., 2012; Lieser et al., 2014).

Yue et al. (2014) proposed that the absence of thrust post-seismic activity within the shallow coseismic large slip areas is consistent with complete stress release in the shallow part of the interplate boundary. However, they ignore the possibility of aseismic afterslip (Lange et al., 2014) at the base of the accretionary prism, which impeded the earthquake from breaching the surface (Scholz, 1998). In addition, Yue et al. (2014) interpretation suggests a stick-slip behaviour for the shallower portion of the interplate boundary as the deeper zone of the seismogenic contact. Alternatively, the absence of aftershocks activity is also consistent with a velocity strengthening frictional behaviour and conditionally stable frictional behaviour for the frontal and middle prisms, respectively (Scholz, 1998). In this alternative interpretation, the interplate boundary below the accretionary prism, has a creeping behaviour during the interseismic period, but it is activated during large earthquakes in response to the slip velocity jumps associated to the rupture nucleated at deeper unstable zones (Scholz, 1998). An interesting implication of this interpretation is that the relatively large slip near the trench associated to the Maule earthquake could not prevent tsunamigenic sources during future earthquakes of moderate magnitude ($M_w \sim 8$) in the area. Thus, the lack of thrust aftershocks at the base of the accretionary prism is likely controlled by the little slip deficit, but also by the rheology of the accretionary prism in the shallow part of the plate boundary. Nevertheless, interpretations are extremely sensitive to the accuracy of the geodetic coseismic slip models, the detection of creeping zones such as slow slip events and the uncertainties of which are particularly high offshore. Thus offshore geodetic data of high resolution are necessary to resolve whether aftershocks are located preferentially in areas of low slip or not.

Acknowledgements

This work was supported by the Chilean National Science Foundation FONDECYT grant 1130004. Sonderforschungsbereich 574 (Special Research Area) “Volatiles and Fluids in Subduction Zones”, funded by the German Research Foundation, enabled acquisition of seismic data and contributed to the bathymetric map. A. Maksymowicz acknowledges the support of the FONDECYT grant 3150160. We thank the Editor Peter Shearer, Stephen Hicks, and an anonymous reviewer for their careful reviews of the manuscript.

Appendix A. Supplementary material

Supplementary material related to this article can be found online at <http://dx.doi.org/10.1016/j.epsl.2017.08.028>.

References

- Angermann, D., Klotz, J., Reigber, C., 1999. Space geodetic estimation of the Nazca South America Euler vector. *Earth Planet. Sci. Lett.* 171 (3), 329–334.
- Bangs, N.L., Cande, S.C., 1997. Episodic development of a convergent margin inferred from structures and processes along the southern Chile margin. *Tectonics* 16 (3), 489–503.
- Byrne, D.E., Davis, D.M., Sykes, L.R., 1988. Loci and maximum size of thrust earthquakes and the mechanics of the shallow region of subduction zones. *Tectonics* 7 (4), 833–857.
- Clift, P., Vannucchi, P., 2004. Controls on tectonic accretion versus erosion in subduction zones: implications for the origin and recycling of the continental crust. *Rev. Geophys.* 42, RG2001. <http://dx.doi.org/10.1029/2003RG000127>.
- Contardo, X., Cembrano, J., Jensen, A., Díaz Naveas, J., 2008. Tectono-sedimentary evolution of marine slope basins in the Chilean forearc (33°30′–36°50′S): insights into their link with the subduction process. *Tectonophysics* 459 (1–4), 206–218.
- Contreras-Reyes, E., Flueh, E.R., Grevemeyer, I., 2010. Tectonic control on sediment accretion and subduction off south central Chile: implications for coseismic rupture processes of the 1960 and 2010 megathrust earthquakes. *Tectonics* 29, TC6018. <http://dx.doi.org/10.1029/2010TC002734>.
- Contreras-Reyes, E., Voelker, D., Bialas, J., Moscoso, E., Grevemeyer, I., 2016. Reloca Slide: an ~ 24 km³ submarine mass wasting event in response to oversteepening and failure of the central Chilean continental slope. *Terra Nova* 28, 257–264. <http://dx.doi.org/10.1111/ter.12216>.
- Cubas, N., Avouac, J.P., Soulomiac, P., Leroy, Y., 2013. Megathrust friction determined from mechanical analysis of the forearc in the Maule earthquake area. *Earth Planet. Sci. Lett.* 381, 92–103.
- Delouis, B., Nocquet, J.-M., Valle, M., 2010. Slip distribution of the February 27, 2010 $M_w = 8.8$ Maule Earthquake, central Chile, from static and high-rate GPS, InSAR, and broadband teleseismic data. *Geophys. Res. Lett.* 37, L17305.
- DeMets, C., Gordon, R.G., Argus, D.F., 2010. Geologically current plate motions. *Geophys. J. Int.* 181 (1), 1–80.
- Dominguez, S., Malavielle, J., Lallemand, S.E., 2000. Deformation of accretionary wedges in response to seamount subduction: insights from sandbox experiments. *Tectonics* (ISSN 0278-7407) 19. <http://dx.doi.org/10.1029/1999TC900055>.
- Fujii, Y., Satake, K., 2013. Slip distribution and seismic moment of the 2010 and 1960 Chilean earthquakes inferred from tsunami waveforms and coastal geodetic data. *Pure Appl. Geophys.* 170, 1493–1509. <http://dx.doi.org/10.1007/s00024-012-0524-2>.
- Fujiwara, T., et al., 2011. The 2011 Tohoku-Oki earthquake: displacement reaching the trench axis. *Science* 334, 1240.
- Glodny, J., et al., 2006. Long-term geological evolution and mass-flow balance of the South-Central Andes. In: Oncken, O., et al. (Eds.), *The Andes: Active Subduction Orogeny*. In: *Frontiers in Earth Science*, vol. 3. Springer, Berlin, pp. 401–428.
- Gulick, S.P.S., et al., 2011. Updip rupture of the 2004 Sumatra earthquake extended by thick indurated sediments. *Nat. Geosci.* 4, 453–456.
- Hicks, S.P., Rietbrock, A., Ryder, I.M.A., Lee, C.-S., Miller, M., 2014. Anatomy of a megathrust: the 2010 M_w 8.8 Maule, Chile earthquake rupture zone imaged using seismic tomography. *Earth Planet. Sci. Lett.* 405, 142–155. <http://dx.doi.org/10.1016/j.epsl.2014.08.028>.
- Kodaira, S., et al., 2012. Coseismic fault rupture at the trench axis during the 2011 Tohoku-oki earthquake. *Nat. Geosci.* 5 (9), 646–650. <http://dx.doi.org/10.1038/ngeo1547>.
- Kopp, H., Klaeschen, D., Flueh, E.R., Bialas, J., Reichert, C., 2002. Crustal structure of the Java margin from seismic wide-angle and multichannel reflection data. *J. Geophys. Res.* 107, B2. <http://dx.doi.org/10.1029/2000JB000095>.
- Korenaga, J., Holbrook, W., Kent, G., Kelemen, P., Detrick, R., Larsen, H.-C., Hopper, J., Dahl-Jensen, T., 2000. Crustal structure of the southeast Greenland margin from joint refraction and reflection seismic tomography. *J. Geophys. Res.* 105 (B9), 21591–21614.
- Kukowski, N., Oncken, O., 2006. Subduction erosion: the “normal” mode of forearc material transfer along the Chilean margin? In: Oncken, O., et al. (Eds.), *The Andes: Active Subduction Orogeny*. In: *Frontiers in Earth Science*, vol. 3. Springer, Berlin, pp. 217–236.
- Lange, D., Tilmann, F., Barrientos, S., Contreras-Reyes, E., Methe, P., Moreno, M., Heit, B., Agurto, H., Bernard, P., Vilotte, J.-P., Beck, S., 2012. Aftershock seismicity of the 27 February 2010 M_w 8.8 Maule earthquake rupture zone. *Earth Planet. Sci. Lett.* 317–318, 413–425. <http://dx.doi.org/10.1016/j.epsl.2011.11.034>.
- Lange, D., Bedford, J.R., Moreno, M., Tilmann, F., Baez, J.C., Bevis, M., Krueger, F., 2014. Comparison of postseismic afterslip models with aftershock seismicity for three subduction-zone earthquakes: Nias 2005, Maule 2010 and Tohoku 2011. *Geophys. J. Int.* 199, 784–799.
- Lange, D., Geersen, J., Barrientos, S., Moreno, M., Grevemeyer, I., Contreras-Reyes, E., Kopp, H., 2016. Aftershock seismicity and tectonic setting of the 16 September 2015 M_w 8.3 Illapel earthquake, Central Chile. *Geophys. J. Int.* 206, 1424–1430. <http://dx.doi.org/10.1093/gji/ggw218>.
- Laursen, J., Scholl, D.W., von Huene, R., 2002. Neotectonic deformation of the central Chile margin: deepwater forearc basin formation in response to hot spot ridge and seamount subduction. *Tectonics* 21 (5), 1038. <http://dx.doi.org/10.1029/2001TC901023>.
- Lay, T., Ammon, C.J., Kanamori, H., Koper, K.D., Sufri, O., Hutko, A.R., 2010. Teleseismic inversion for rupture process of the 27 February 2010 Chile ($M_w = 8.8$) earthquake. *Geophys. Res. Lett.* 37, L13301. <http://dx.doi.org/10.1029/2010GL043379>.
- Lieser, K., Grevemeyer, I., Lange, D., Flueh, E., Tilmann, F., Contreras-Reyes, E., 2014. Splay fault activity revealed by aftershocks of the 2010 M_w 8.8 Maule earthquake, central Chile. *Geology* 42, 823–826. <http://dx.doi.org/10.1130/G35848.1>.
- Lin, Y.-n.N., et al., 2013. Coseismic and postseismic slip associated with the 2010 Maule Earthquake, Chile: characterizing the Arauco Peninsula barrier effect. *J. Geophys. Res.*, Solid Earth 118, 3142–3159. <http://dx.doi.org/10.1002/jgrb.50207>.
- Lorito, S., Romano, F., Atzori, S., Tong, X., Avallone, A., McCloskey, J., Cocco, M., Boschi, E., Piatanesi, A., 2011. Limited overlap between the seismic gap and coseismic slip of the great 2010 Chile earthquake. *Nat. Geosci.* 4, 173–177.

- Maksymowicz, A., 2015. The geometry of the Chilean continental wedge: tectonic segmentation of subduction processes of Chile. *Tectonophysics* 659, 183–196. <http://dx.doi.org/10.1016/j.tecto.2015.08.007>.
- Maksymowicz, A., Trehu, A., Contreras-Reyes, E., Ruiz, S., 2015. Density-depth model of the continental wedge at the maximum slip segment of the Maule Mw8.8 megathrust earthquake. *Earth Planet. Sci. Lett.* 409, 265–277. <http://dx.doi.org/10.1016/j.epsl.2014.11.005>.
- Maksymowicz, A., Chadwell, D., Ruiz, J., Tréhu, A., Contreras-Reyes, E., Weinrebe, W., Díaz-Naveas, J., Gibson, J.C., Lonsdale, P., Tryon, M.D., 2017. Coseismic seafloor deformation in trench region during the Maule Mw8.8 megathrust earthquake. *Sci. Rep.*. <http://dx.doi.org/10.1038/srep45918>.
- Moreno, M., et al., 2012. Toward understanding tectonic control on the Mw 8.8, Maule Chile earthquake. *Earth Planet. Sci. Lett.* 321, 152–165.
- Moreno, M., Bolte, J., Klotz, J., Melnick, D., 2009. Impact of megathrust geometry on inversion of coseismic slip from geodetic data: application to the 1960 Chile earthquake. *Geophys. Res. Lett.* 36, L16310. <http://dx.doi.org/10.1029/2009GL039276>.
- MoscOSO, E., Grevemeyer, I., Contreras-Reyes, E., Flueh, E.R., Dzierma, Y., Rabbel, W., Thorwart, M., 2011. Revealing the deep structure and rupture plane of the 2010 Maule, Chile earthquake (Mw = 8.8) using wide angle seismic data. *Earth Planet. Sci. Lett.* 307, 147–155. <http://dx.doi.org/10.1016/j.epsl.2011.04.025>.
- MoscOSO, E., Grevemeyer, I., 2015. Bending related faulting of the incoming oceanic plate and its effect on lithospheric hydration and seismicity: a passive and active seismological study offshore Maule: Chile. *J. Geodyn.* 90, 58–70. <http://dx.doi.org/10.1016/j.jog.2015.06.007>.
- Pietrzak, et al., 2007. Defining the source region of the Indian Ocean Tsunami from GPS, altimeters, tide gauges and tsunami models. *Earth Planet. Sci. Lett.* 261, 1–2. <http://dx.doi.org/10.1016/j.epsl.2007.06.002>. 49–64.
- Plafker, G., Savage, J., 1970. Mechanism of the Chilean earthquake of May 21 and 22, 1960. *Geol. Soc. Am. Bull.* 81, 1001–1030.
- Rietbrock, A., Ryder, I., Hayes, G., Haberland, C., Comte, D., Roecker, S., Lyon-Caen, H., 2012. Aftershock seismicity of the 2010 Maule Mw = 8.8, Chile, earthquake: correlation between coseismic slip models and aftershock distribution? *Geophys. Res. Lett.* 39, L08310. <http://dx.doi.org/10.1029/2012GL051308>.
- Saffer, D.M., Marone, C., 2003. Comparison of smectite- and illite-rich gouge frictional properties: application to the updip limit of the seismogenic zone along subduction megathrusts. *Earth Planet. Sci. Lett.* 215, 219–235. [http://dx.doi.org/10.1016/S0012-821X\(03\)00424-2](http://dx.doi.org/10.1016/S0012-821X(03)00424-2).
- Sakaguchi, A., et al., 2011. Seismic slip propagation to the updip end of plate boundary subduction interface faults: vitrinite reflectance geothermometry on Integrated Ocean Drilling Program NanTro SEIZE cores. *Geology* 39, 395–398.
- Scholz, C.H., 1998. Earthquakes and friction laws. *Nature* 391 (6662), 37–42.
- Shinohara, M., et al., 2012. Precise aftershock distribution of the 2011 off the Pacific coast of Tohoku Earthquake revealed by an ocean-bottom seismometer network. *Earth Planets Space* 64, 8. <http://dx.doi.org/10.5047/eps.2012.09.003>.
- Simons, M., et al., 2011. The 2011 magnitude 9.0 Tohoku-Oki earthquake: missing the megathrust from seconds to centuries. *Science* 332, 1421. <http://dx.doi.org/10.1126/science.1206731>.
- Vigny, C., et al., 2011. The 2010 Mw 8.8 Maule megathrust earthquake of Central Chile, monitored by GPS. *Science* 332, 1417–1421.
- Tilmann, F., Craig, T., Grevemeyer, I., Suwargadi, B., Kopp, H., Flueh, E., 2010. The updip seismic/aseismic transition of the Sumatmegathrust illuminated by aftershocks of the 2004 Aceh-Andaman and 2005 Nias events. *Geophys. J. Int.* 181 (3), 1261–1274.
- Trehu, A., Tryon, M., 2012. MV1206 Cruise Report, Structure of the Accretionary Prism Updip of the M8.8 Maule Earthquake Rupture. www.rvdata.org/MV1206.
- Yue, H., et al., 2014. Localized fault slip to the trench in the 2010 Maule, Chile Mw = 8.8 earthquake from joint inversion of high-rate GPS, teleseismic body waves, InSAR, campaign GPS, and tsunami observations. *J. Geophys. Res.* 119. <http://dx.doi.org/10.1002/2014JB011340>.
- Voelker, D., Scholz, F., Geersen, J., 2011. Analysis of submarine landsliding in the rupture area of the 27 February 2010 Maule earthquake, Central Chile. *Mar. Geol.* 288, 79–89.
- von Huene, R., Ranero, C.R., Scholl, D.W., 2009. Convergent margin structure in high-quality geophysical images and current kinematic and dynamic models. In: Lallemand, S., Funicello, F. (Eds.), *Subduction Zone Geodynamics*. In: *Frontiers in Earth Sciences*, vol. 137. Springer, Berlin, pp. 137–157.
- Wang, K., Hu, Y., 2006. Accretionary prisms in subduction earthquake cycles: the theory of dynamic Coulomb wedge. *J. Geophys. Res.* 111, B06410. <http://dx.doi.org/10.1029/2005JB004094>.
- Wells, R.E., Blakely, R.J., Sugiyama, Y., Scholl, D.W., Dinterman, P.A., 2003. Basin-centered asperities in great subduction zone earthquakes: a link between slip, subsidence, and subduction erosion? *J. Geophys. Res.* 108 (B10), 250. <http://dx.doi.org/10.1029/2002JB002072>.
- Zelt, C.A., 1999. Modelling strategies and model assessment for wide-angle seismic traveltimes data. *Geophys. J. Int.* 139, 183–204. <http://dx.doi.org/10.1046/j.1365-246X.1999.00934.x>.